Peer Reviewed
2015 Solar Research Conference

2015 ASIA-PACIFIC
SOLAR RESEARCH CONFERENCE

Temperature and Heat Flux Distributions in Sodium Receiver Tubes

William Logie, Charles-Alexis Asselineau, John Pye and Joe Coventry

Solar Thermal Group
The Australian National University, Canberra
E-mail: will.logie@anu.edu.au

Abstract

This paper presents an analysis of tube wall heat transfer using a simplified two-dimensional model. Wall conduction is modelled using the `laplacianFoam` solver from OpenFOAM® with boundary conditions representing internal/external convection and radiation. Using this model, the effect of sodium as a working fluid is compared with molten salt, and tube performance is characterised through the use of tube efficiency. Fouling has a significant effect on the efficiency with molten salt as a heat transfer fluid. Variation in fluid flow parameters and tube dimensions also have a significant impact on the efficiency tubes using molten salt. Tubes using liquid sodium are effectively insensitive to tube diameter and flow velocity.

1 Introduction

Tubular receivers are commonly used at the focus of high-temperature solar thermal systems. Concentrated solar flux incident on the tubes is absorbed and then conducted through the tubes to the working fluid flowing inside. In heat exchanger and boiler systems, the heat transfer through the tubes may be considered uniform around the tube perimeter, however in concentrating solar power (CSP) applications, the irradiance on the tubes is highly asymmetric, and effectively only a portion of the tube perimeter may be participating in the transfer of heat from the outside to the inside surface. This limited area reduces the performance of the receiver: the temperature difference across the tube and across the internal convection boundary layer is increased, and the higher external surface temperature means that radiative and convective losses in this area are too.

Prior work has been particularly focused on tubular receivers where air, thermal oil, water, or molten salt is the working fluid. Many works of late have explored how receiver efficiency and tube stresses vary with tube dimensions. Current consensus for example is that the peak allowable flux for tubes carrying water/steam lies in the region 0.3–0.7 MW/m^2 and for molten salt up to 1.0 MW/m^2 (Liao *et al.* , 2014; Rodríguez-Sánchez *et al.* , 2014). The constraint is largely one of thermal elastic tube stress, but also in the case of molten salt, the temperature at which decomposition occurs ($\approx$ 580 °C). Of particular interest here is the case of sodium as the working fluid (Schiel & Geyer, 1988; Boerema *et al.* , 2013). Sodium has very high

conductivity and it is unclear whether the same material limitations will apply, since boundary layer temperature difference is far lower than for molten salt, and high temperature corrosion of the tube can be controlled (Pacio *et al.* , 2013; Fernandes *et al.* , 1994).

In constructing a model to eventually include the thermal elasticity of the tubes, it is essential to determine heat flux and temperature distribution accurately. Simple one-dimensional analysis can provide satisfactory information when observing only thermodynamics, but if material stress, strain and deformation is also to be determined, one needs to model the second and perhaps third dimension as well. While it is desirable to model the conjugate heat transfer between fluid and solid with validated computational fluid dynamics (CFD) (Yang *et al.* , 2012; Flesch *et al.* , 2014), much at this point can be deduced by observing the solid tube region with von Neumann boundary conditions.

2 Model

Conduction through the tube is calculated on a structured hexahedral mesh according to the heat equation:

$$\frac{\partial T}{\partial t} - \kappa \nabla^2 T = 0, \tag{1}$$

in which temperature T varies as a function of time t and according to the material thermal diffusivity κ of a defined space subject to sinks and sources on boundaries. The Laplacian ∇^2 operates on two-dimensions (x and y) in the context of this paper, however extension to the third dimension (z) in OpenFOAM® is easily implemented in the mesh generation step.

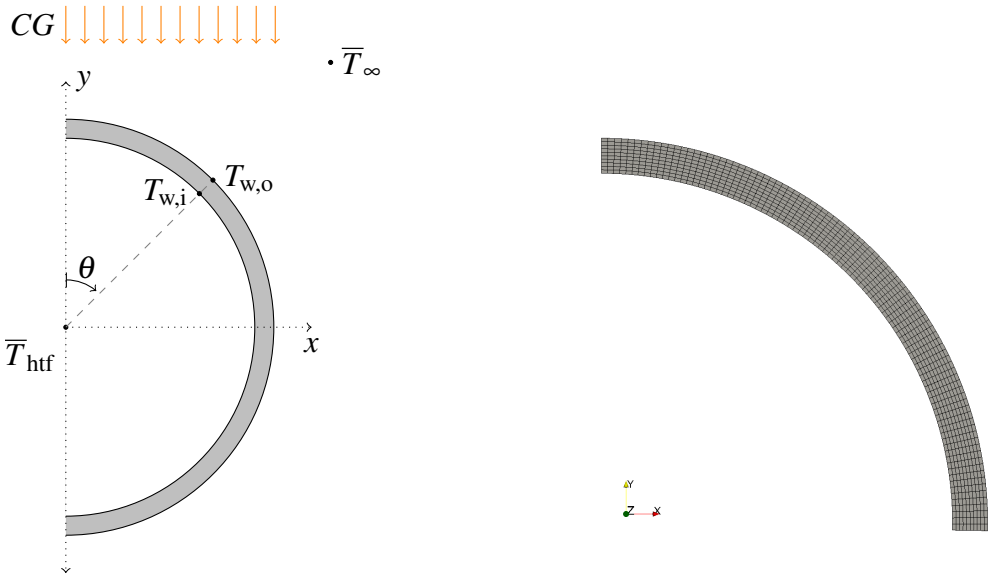

(a) Model notation **(b)** Irradiated quadrant of tube mesh

Figure 1: Simple two-dimensional model

To begin with, we observe the intensity distribution of collimated incident flux on half a tube assuming symmetry about its middle (y-axis), as illustrated in Figure 1a. The energy balance at

the outer tube wall is calculated for each discrete surface element according to Eq. 3:

$$k_{\mathrm{w}} \left.\frac{\partial T}{\partial n}\right|_{\mathrm{w,o}} = q''_{\mathrm{w,o}} = q''_{\mathrm{incident}} - q''_{\mathrm{loss,rad}} - q''_{\mathrm{loss,conv}} \tag{2}$$

$$= \alpha C G \cos(\theta) - \varepsilon\sigma(T^4_{\mathrm{w,o}} - \overline{T}^4_{\infty}) - \overline{h}_{\mathrm{o}}(T_{\mathrm{w,o}} - \overline{T}_{\infty}) \tag{3}$$

This operates on the outer boundary of the tube by setting the wall-normal temperature gradient $\frac{\partial T}{\partial n}$ to the first cell according to thermal conductivity of the wall k_{w} as the irradiation heat flux (concentration ratio $C = 800$ and solar constant $G = 1000$ W/m^2) is attenuated by absorption coefficient $\alpha = 0.968$ (Pye *et al.* , 2014), incident angle $\cos(\theta)$, re-radiation where σ is the Stefan-Boltzmann constant and $\varepsilon \approx 0.87$ (Ho *et al.* , 2012), and an average external convection loss $\overline{h}_{\mathrm{o}} = 30$ W$/$(m^2.K), which accounts for a little wind (Siebers & Kraabel, 1984; Pye *et al.* , 2014)[1].

Heat transfer to the fluid can be calculated with Nusselt correlations evaluated by way of cross sectional area A'_{i}, flow velocity U and Reynolds Number using temperature dependent thermo-physical properties (density ρ, specific heat c_{p}, molecular viscosity μ and thermal conductivity k)[2] for molten salt (Zavoico, 2001) and liquid sodium (Fink & Leibowitz, 1995):

$$A'_{\mathrm{i}} = \pi \left(\frac{d_{\mathrm{i}}}{2}\right)^2 \tag{4}$$

$$U = \frac{\dot{m}}{A'_{\mathrm{i}}\rho} \tag{5}$$

$$\mathrm{Re} = \frac{U d_{\mathrm{i}}}{\nu}. \tag{6}$$

For liquids with $0.7 \leq \mathrm{Pr} \leq 16{,}700$ the impact of temperature difference in the thermal boundary can be captured in the ratio of bulk fluid to inner tube wall molecular viscosity by way of the Sieder and Tate correlation (Incropera *et al.* , 2006) with all properties other than $\mu_{\mathrm{w,i}}$ evaluated at the bulk fluid temperature:

$$\mathrm{Nu} = 0.027 \mathrm{Re}^{\frac{4}{5}} \mathrm{Pr}^{\frac{1}{3}} \left(\frac{\mu_{\mathrm{htf}}}{\mu_{\mathrm{w,i}}}\right)^{0.14}, \tag{7}$$

or disregarding the thermal boundary layer (viscosity ratio) with the Dittus-Boelter equation:

$$\mathrm{Nu} = 0.023 \mathrm{Re}^{\frac{4}{5}} \mathrm{Pr}^{0.3}. \tag{8}$$

Concealed in both Eqs. 7 and 8 is the assumption that the ratio of hydrodynamic-to-thermal viscosity (Pr) is independent of flow condition and distance from wall. Liquid metals, however, have a high thermal conductivity and very low Prandtl numbers (Pr≈ 0.01 or less), which means that the thermal boundary layer is much thicker than the hydrodynamic boundary layer and is characterised by molecular conduction until Re$> 214{,}000$ (Pacio *et al.* , 2015). The assumption

[1] The case of no-wind is closer to 10 W$/$(m^2.K)

[2] From there we can calculate kinematic viscosity $\nu = \frac{\mu}{\rho}$, thermal diffusivity $\kappa = \frac{k}{\rho c_{\mathrm{p}}}$ and Prandtl Number $\mathrm{Pr} = \frac{\nu}{\kappa}$.

of the Reynolds analogy - that the turbulent Prandtl number $\mathrm{Pr_t}$ is constant and close to unity - cannot be applied, and while a number of empirical models have adapted correlations such as the Lyon-Martinelli to suit $\mathrm{Pr_t} \approx 1-2.5$, their reliability is yet to be confirmed. Short of CFD, the best fit from Pacio *et al.* (2015) will be used with properties evaluated at the bulk fluid temperature according to the Skupinshi, Tortel and Vautrey correlation (Holman, 1997):

$$\mathrm{Nu} = 4.82 + 0.0185(\mathrm{RePr})^{0.827}, \tag{9}$$

which is valid for Reynolds numbers up to 1×10^5. Equation 7 is implemented with a linear fit of convection coefficient to inner wall temperature for any given bulk fluid temperature.

Fouling resistance R_f is added to the convective heat transfer coefficient h_i according to Eq. 11:

$$h_\mathrm{i} = \frac{\mathrm{Nu}k_\mathrm{htf}}{d_\mathrm{i}} \tag{10}$$

$$h_\mathrm{f,i} = \frac{1}{R_\mathrm{f} + \frac{1}{h_\mathrm{i}}}, \tag{11}$$

and heat transfer to the fluid at a bulk temperature $\overline{T}_\mathrm{htf}$ is calculated for each inner discrete surface temperature $T_\mathrm{w,i}$ according to Eq. 12:

$$k_\mathrm{w} \left.\frac{\partial T}{\partial n}\right|_\mathrm{w,i} = q''_\mathrm{w,i} = q''_\mathrm{htf} = h_\mathrm{f,i}(\overline{T}_\mathrm{htf} - T_\mathrm{w,i}). \tag{12}$$

Rodríguez-Sánchez *et al.* (2014) gives the fouling factor R_f for molten salt as 8.808×10^{-5} $\mathrm{m^2}$.K/W, which is the same value given by Zavoico (2001) (5×10^{-4} $\mathrm{ft^2}$.°F.hr/btu) and is very close to that used for pipes carrying steam (Holman, 1997). Fouling in the case of liquid sodium is negligible if impurities such as oxygen are kept below a few ppm (Pacio *et al.* , 2013; Fernandes *et al.* , 1994).

It would be wise to include the effects of coatings such as Pyromark®, however recent measurements of Pyromark's thermal conductivity by Boubault *et al.* (2013) conflict with that published by Schiel *et al.* (1987). The former points to a rather small thermal contact resistance of 2.57×10^{-6} $\mathrm{m^2}$.K/W and conductivity of 6.26 W/(m.K), whereas the latter assumes a thermal conductivity for vitrified silica in the range of 0.6–1.8 W/(m.K) which has been used more broadly for model validation (Boerema *et al.* , 2013). Its effect on radiation losses (external tube temperature) is of secondary importance for the analysis presented here and will be ignored until a more rigorous study can be made.

3 Results

For a given heat transfer fluid and receiver design there is an optimal compromise between tube diameter, tube thickness, temperature increase along the receiver, mass flow through the receiver, maximum tube temperature (thermal-elastic stress) and overall pressure drop. Ideally one seeks to minimise the tube inner diameter so as to maximise forced convective heat transfer, however this is detrimental to pressure-drop and pump cost.

Table 1: Fluid and tube specific properties taken from Pye *et al.* (2014) and evaluated for a bulk fluid temperature of 450 °C

			Molten Salt	Liquid Sodium
Density	ρ	kg/m^3	1804	846
Specific heat	c_p	J/(kg.K)	1520	1272
Molecular viscosity	μ	mPa.s	1.47	0.25
Conductivity	k	W/(m.K)	0.53	66.77
Inner tube diameter	d_i	mm	18	20
Tube wall thickness	t_w	mm	1	1
Mass flow	$\dot{m}$	kg/s	1.60	1.76
Bulk velocity	U	m/s	3.49	6.62
Reynolds Number	Re	-	76864	440332
Pressure drop	ΔP	Pa/m	-11591	-12461
Nusselt Number	$\overline{\text{Nu}}$	-	332	15
Convection coefficient	$\overline{h}_i$	kW/(m^2.K)	9.75	49.29

Pye *et al.* (2014) optimised tube bank receivers for a number of working fluids on the basis of exergy. A summary of these fluid and tube properties are given in Table 1 and will serve as a basis for comparison.

In Figure 2, in which grey shows a negative deviation from the values in Table 1 (white is positive), convective heat transfer coefficient $\overline{h}_i$ is plotted as a function of inner tube diameter d_i, mass flow $\dot{m}$ and bulk fluid temperature $\overline{T}_{htf}$. The Skupinshi correlation estimates convection

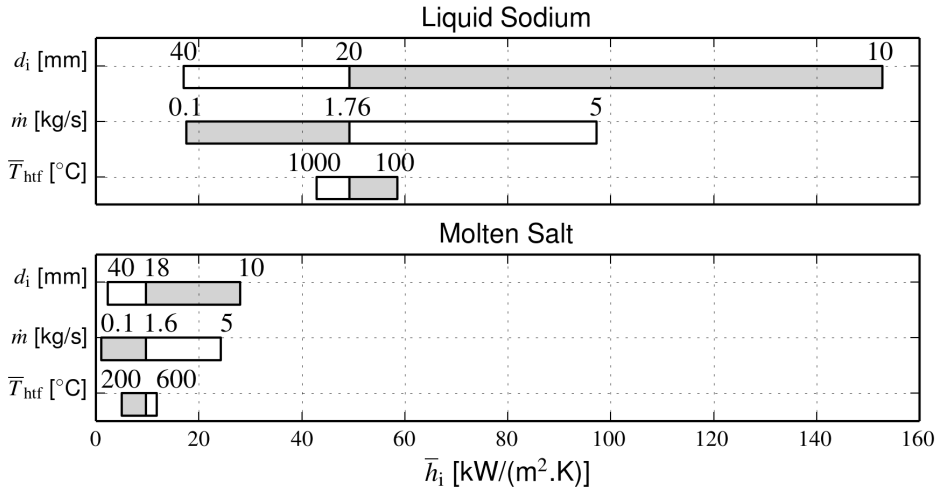

Figure 2: Tornado chart showing the dependency of convective heat transfer coefficient $\overline{h}_i$ on tube diameter d_i, mass flow $\dot{m}$ and bulk fluid temperature $\overline{T}_{htf}$ for both liquid sodium and molten salt

lower than other well known models such as the Lyon-Martinelli, which over-predict without adjustment for Pr_t (Pacio *et al.* , 2015)[3]. In general we observe that an increase in temperature

[3]For the case of sodium where $d_i = 20$ mm, $\dot{m} = 1.76$ kg/s and $\overline{T}_{htf} = 450$ °C, the Lyon-Martinelli equation

improves convection for molten salt, whereas for sodium the convection coefficient decreases. For similar mass flows sodium incurs slightly more pressure drop. This is due to the lower density of sodium, but what is less obvious is that it is not as penalised as one expects, owing to it having a lower viscosity than molten salt. In Figure 3 the dependency of pressure drop in one metre of tube is plotted as a function of the same parameters as in Figure 2.

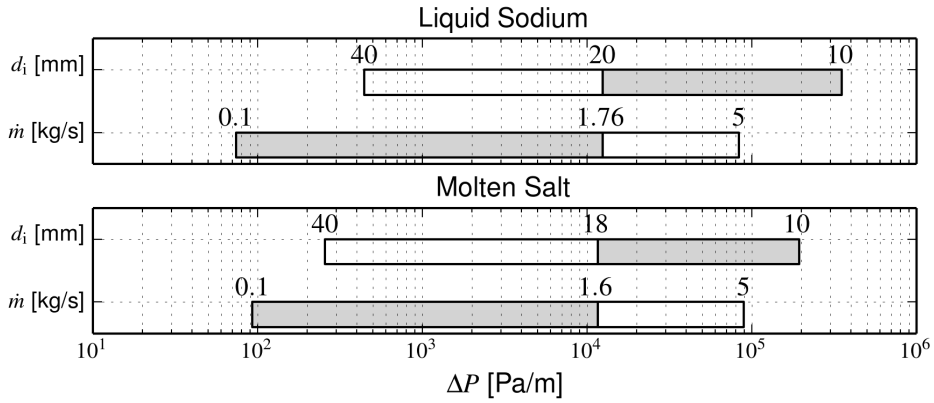

Figure 3: Tornado chart showing the dependency of pressure drop on tube diameter d_i and mass flow $\dot{m}$ for both liquid sodium and molten salt

With boundary conditions set as above in steady-state-seeking simulations in OpenFOAM®, we can extract information about temperatures and heat flux in some post-processing samples. It is apparent in Figure 4 that fouling plays a very significant role in the case of molten salt.

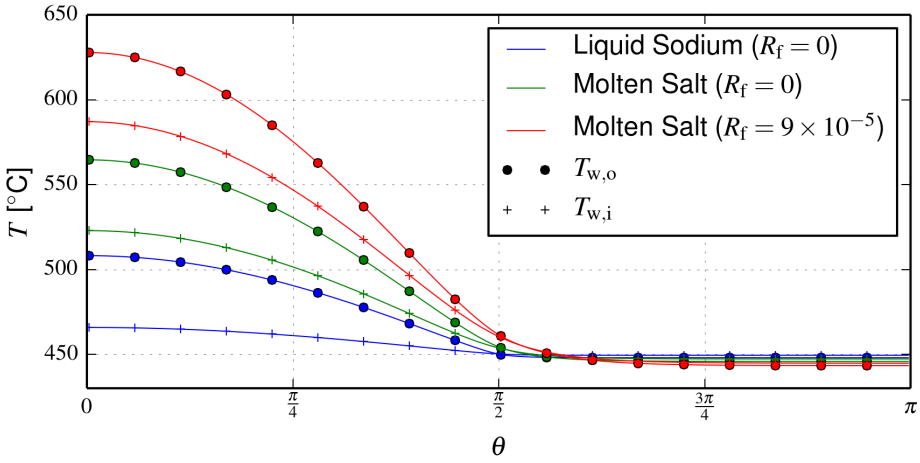

Figure 4: Circumferential temperature of an Inconel® 625LCF tube irradiated with $CG = 800$ kW/m^2

It effectively reduces the convection coefficient by as much as half and significantly raises the temperature of the tube most exposed to irradiance, in this case by around 70 °C, to 592 °C. The maximum inner wall temperature for sodium assuming no fouling is 465 °C.

estimates around 65 kW/(m^2.K)

The overall performance of tubes can be explored better if we introduce tube efficiency according to Eq. 13:

$$\eta_{\text{tube}} = \frac{d_{\text{i}} \int_0^{\pi} q''_{\text{htf}} \mathrm{d}\theta}{d_{\text{o}} \int_0^{\pi} q''_{\text{incident}} \mathrm{d}\theta}. \tag{13}$$

If we observe the same variation in tube diameter and mass flow as was illustrated in Figure 2, the sensitivity of tube efficiency is shown in Figure 5 instead of heat transfer coefficient, and the real fouling factor of $R_{\text{f}} = 9 \times 10^{-5}$ is used for molten salt. Due to its high conductivity,

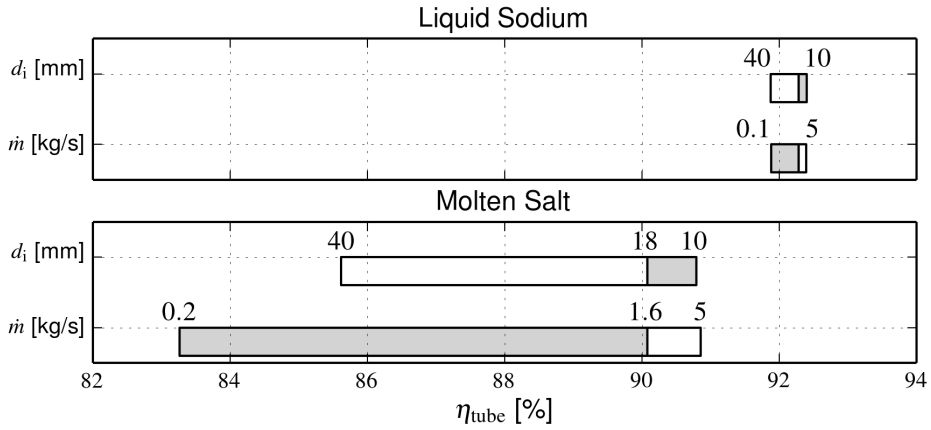

Figure 5: Tornado chart showing the dependency of Inconel® 625LCF tube efficiency on tube diameter d_{i} and mass flow $\dot{m}$ for both liquid sodium and molten salt

liquid sodium is effectively insensitive to a large range of tube diameters and mass flows; tube efficiency is not impacted to the same degree as molten salt. This realisation makes the exploration of receiver design with liquid sodium much less restricted, as it is much harder to penalise efficiency of the tubes or whichever other volumetric bodies are investigated.

It is interesting to note that sodium still performs well with a tube thickness up to 2 mm, as seen in Figure 7. In considering liquid sodium as a prospective heat transfer fluid, we must be sure that tubes do not fail. This may require tubes having additional thickness.

4 Conclusion

A case has been developed in OpenFOAM® for the purpose of observing temperature and heat transfer in tubes carrying molten salt and liquid sodium.

The impact of fouling from corrosion on tube temperature is significant and further clarification of it is required, in particular confirmation of the nature of corrosion under the design conditions sought. Thermal characterisation of Pyromark® is also required to better capture external tube surface temperature.

The tube efficiency of liquid sodium is effectively insensitive to a huge range of dimensions and operating conditions owing to its high thermal conductivity.

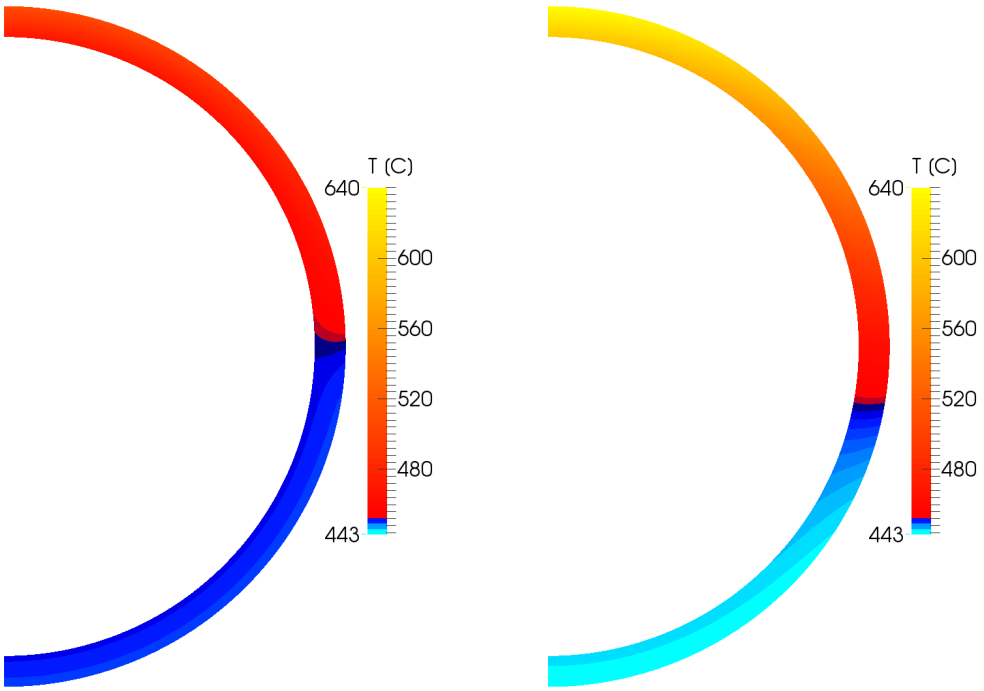

(a) Liquid Sodium **(b)** Molten Salt

Figure 6: Screenshots from ParaView showing tube temperature with molten salt and liquid sodium as in Table 1

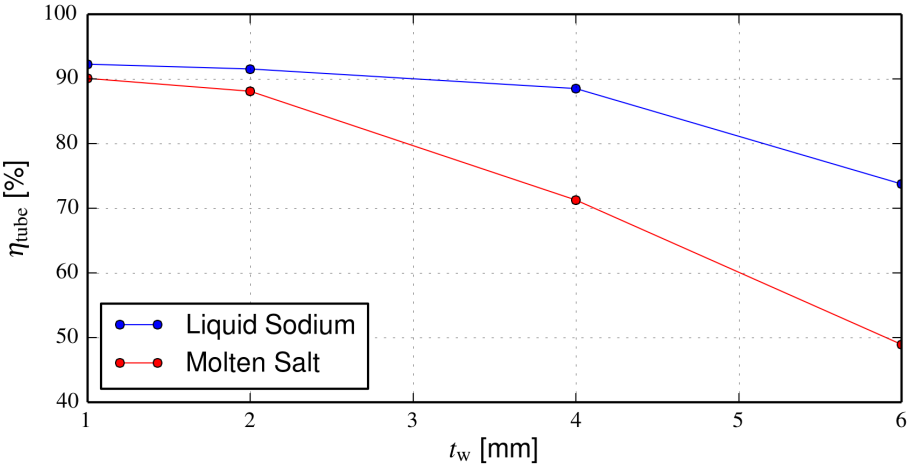

Figure 7: Plot of Inconel® 625LCF tube efficiency for both liquid sodium and molten salt with increasing tube thickness

5 Outlook

Further development of the model to include incident ray-tracing profiles, re-radiation models (e.g. Radiosity) and CFD for the heat transfer fluid (Marocco *et al.* , 2014) will endeavour to resolve the problem further. Accurate resolution of the tube temperatures is required to observe thermal-elastic stress, strain and viso-elastic relaxation[4] of next-generation sodium receiver designs. This next phase of model development will make use of the Fluid Structure Interaction package, which has already been successfully validated with an analytical case from Timoshenko & Goodier (1951).

6 Acknowledgements

Many of the findings presented in this paper draws on research performed as part of the Australian Solar Thermal Research Initiative (ASTRI), a project supported by the Australian Government, through the Australian Renewable Energy Agency (ARENA). Responsibility for the views, information or advice expressed herein is not accepted by the Australian Government. The corresponding author is supported by an Australian Postgraduate Award.

References

BOEREMA, N., MORRISON, G., TAYLOR, R., & ROSENGARTEN, G. 2013. High temperature solar thermal central-receiver billboard design. *Solar Energy*, **97**, 356–368.

BOUBAULT, A., CLAUDET, B., FAUGEROUX, O., & OLALDE, G. 2013. Accelerated aging of a solar absorber material subjected to highly concentrated solar flux. *In: 19th Annual SolarPACES Symposium*. Las Vegas.

FERNANDES, P. J. L., CLEGG, R. E., & JONES, D. R. H. 1994. Failure by liquid metal induced embrittlement. *Engineering Failure Analysis*, **1**(1), 51–63.

FINK, J. K., & LEIBOWITZ, L. 1995. *Thermodynamic and Transport Properties of Sodium Liquid and Vapor*. Tech. rept. ANL/RE-95/2. Reactor Engineering Division, Argonne National Laboratory, Chicago.

FLESCH, J., FRITSCH, A., CAMMI, G., MAROCCO, L., FELLMOSER, F., PACIO, J., & WETZEL, TH. 2014. Construction of a Test Facility for Demonstration of a Liquid Lead-bismuth-cooled 10 kW Thermal Receiver in a Solar Furnace Arrangement - {SOMMER}. *In: 20th Annual SolarPACES Symposium*. Beijing.

HO, C. K., MAHONEY, A. R., AMBROSINI, A., BENCOMO, M., HALL, A., & LAMBERT, T. N. 2012. Characterization of Pyromark 2500 for high-temperature solar receivers. *In: ASME 2012 6th International Conference on Energy Sustainability & 10th Fuel Cell Science*. San Diego.

HOLMAN, J. P. 1997. *Heat Transfer*. 8th edn. McGraw-Hill, Inc.

[4] By way of Prony Series.

INCROPERA, F P, DEWITT, D P, BERGMAN, T L, & LAVINE, A S. 2006. *Fundamentals of Heat and Mass Transfer*. 6th edn. John Wiley & Sons.

LIAO, Z., LI, X., XU, C., CHANG, C., & WANG, Z. 2014. Allowable flux density on a solar central receiver. *Renewable Energy*, **62**, 747–753.

MAROCCO, L., CAMMI, G., FLESCH, J., & WETZEL, TH. 2014. Numerical analysis of a solar tower receiver tube operated with liquid metals. *International Journal of Heat and Mass Transfer*. submitted 28th November.

PACIO, J., SINGER, C., WETZEL, T., & UHLIG, R. 2013. Thermodynamic evaluation of liquid metals as heat transfer fluids in concentrated solar power plants. *Applied Thermal Engineering*, **60**, 295–302.

PACIO, J., MAROCCO, L., & WETZEL, T. 2015. Review of data and correlations for turbulent forced convective heat transfer of liquid metals in pipes. *Heat Mass Transfer*, **51**, 153–164.

PYE, J., ZHENG, M., ZAPATA, J., ASSELINEAU, C.-A., & COVENTRY, J. 2014. An exergy analysis of tubular solar-thermal receivers with different working fluids. *In: 20th Annual SolarPACES Symposium*. Beijing.

RODRÍGUEZ-SÁNCHEZ, M. R., SORIA-VERDUGO, A., ALMENDROS-IBÁÑEZ, J. A., ACOSTA-IBORRA, A., & SANTANA, D. 2014. Thermal design guidelines of solar power towers. *Applied Thermal Engineering*, **63**, 428–438.

SCHIEL, W., GEYER, M., & CARMONA, R. 1987. *The IEA-SSPS high flux experiment - testing the advanced sodium receiver at fluxes up to 2.5 MW/m^2*. Berlin, Heidelberg, New York: Springer-Verlag.

SCHIEL, W. J. C., & GEYER, M. A. 1988. Testing an external sodium receiver up to heat fluxes of 2.5 MW/m^2: results and conclusions from the IEA-SSPS high flux experiment conducted at the central receiver system of the Plataforma Solar De Almeria (Spain). *Solar Energy*, **41**, 255–265.

SIEBERS, D. L., & KRAABEL, J. S. 1984. *Estimating convective energy losses from solar central receivers*. Tech. rept. SAND84-8717. Sandia National Laboratories, Alburquerque.

TIMOSHENKO, S., & GOODIER, J. N. 1951. *Theory of Elasticity*. McGraw-Hill Book Company, Inc.

YANG, X., YANG, X., DING, J., SHAO, Y., & FAN, H. 2012. Numerical simulation study on the heat transfer characteristics of the tube receiver of the solar thermal power tower. *Applied Energy*, **90**, 142–147.

ZAVOICO, A. B. 2001. *Solar power tower design basis document*. Tech. rept. SAND2001-2100 Rev 0. Sandia National Laboratories, California.